Structural Safety 31 (2009) 490–499

Contents lists available at ScienceDirect

Structural Safety

journal homepage: www.elsevier.com/locate/strusafe

Structural optimization for performance-based design in earthquake engineering: Applications of neural networks

Oscar Möller [a], Ricardo O. Foschi [b,*], Laura M. Quiroz [a], Marcelo Rubinstein [a]

[a] Instituto de Mecánica Aplicada y Estructuras IMAE, Universidad Nacional de Rosario, Riobamba y Berutti, 2000 Rosario, Argentina
[b] Department of Civil Engineering, University of British Columbia, 6250 Applied Science Ln., Vancouver V6T 1Z4, Canada

ARTICLE INFO

Article history:
Received 5 June 2008
Received in revised form 13 April 2009
Accepted 30 June 2009
Available online 15 August 2009

Keywords:
Performance-based design
Optimization
Reliability
Neural networks
Earthquake engineering

ABSTRACT

This work addresses an approach to performance-based design in the context of earthquake engineering. The objective is the optimization of the total structural cost, under constraints related to minimum target reliabilities specified for the different limit states or performance requirements. The problem involves (1) the use of a nonlinear, time-stepping dynamic analysis to investigate the responses of relevance to the performances' evaluation and (2) the integration of the responses into measures of damage accumulated during the earthquake. The random responses are deterministically obtained for different combinations of the design parameters and the intervening random variables, of which some are associated with the structure and some with the earthquake characteristics. The approach uses a neural network representation of the responses and, for each one, the variability associated with different earthquake records is accommodated by developing two networks: one for the mean response over the records, and another for the corresponding standard deviation. The neural network representation facilitates the estimation of reliability by Monte Carlo simulation, and the reliability achieved in each performance level, for a specific combination of the design parameters, is itself represented with a neural network. This is then used within an optimization algorithm for minimum total cost under reliability constraints. An application example uses a reinforced concrete, multi-storey plane structure with seismic demands corresponding to the city of Mendoza, Argentina.

0. Introduction

General performance-based design guidelines [1,2] imply an optimization for optimum design parameters, in order to minimize an objective (for example, the total cost of the structure), while maintaining minimum target reliabilities for each desired performance level. Thus, the guidelines imply accounting for the uncertainties in the intervening variables, some related to the structural capacity and others, for seismic demands, to the characteristics of the ground motion.

Reliability calculations for the different performance requirements require the estimation of maximum structural responses over the duration of the earthquake. These responses are generally associated with a strongly nonlinear structural behavior, and must be obtained using a step-by-step nonlinear, numerical dynamic analysis for each earthquake record. As this process could be computationally demanding, reliability estimation via direct Monte Carlo simulation may become an unfeasible proposition. Since it is not possible to establish an explicit relationship between input parameters and dynamic responses, discrete results can be obtained for specific combinations of the intervening random variables and design parameters. In turn, these discrete results can be represented by a response surface or neural network which, when properly adjusted, can be used as a substitute for the dynamic analysis. Neural network applications in civil engineering have been the subject of extensive research, ranging from topics in geotechnical engineering (liquefaction prediction) to the generation of artificial earthquakes. Of particular relevance to the work presented here, neural networks have been used for the representation of structural responses [3–6]. Recent research results have also extended the use of neural network response representations with a focus on structural optimization under uncertainty [7,8].

The present work also considers the problem of structural optimization for earthquake demands under minimum reliability constraints. The approach discussed here involves the following steps: (1) obtaining the response parameters by nonlinear dynamic analyses for a set of combinations of the intervening variables, design parameters and earthquake records; (2) representing, via neural networks, the set of deterministically obtained responses; (3) formulating the different performance criteria in terms of the response parameters; (4) using the neural networks as substitutes for the nonlinear dynamic analysis and calculating, via Monte Carlo

* Corresponding author.
E-mail addresses: moller@fceia.unr.edu.ar (O. Möller), rowfa1@civil.ubc.ca (R.O. Foschi).

0167-4730/$ - see front matter © 2009 Elsevier Ltd. All rights reserved.
doi:10.1016/j.strusafe.2009.06.007

simulation, the reliability achieved for different choices of the design parameters; (5) representing the relationship between reliability level and design parameters via neural networks; (6) optimize the structure, using the neural networks for responses and for reliability to achieve a minimum total cost while satisfying minimum target reliabilities for each performance criterion. The following sections discuss, in turn, each of these steps.

The work adds to previous research in introducing neural networks for the reliability achieved in each limit state as a function of the design parameters, and presenting a simple minimization algorithm based on a gradient-free search.

1. Nonlinear dynamic responses and representation with neural networks

1.1. Brief description of the nonlinear dynamic analysis model

The structural model used here has been discussed in more detail elsewhere [9,10] and only a brief description is given here. It considers the frame as a set of one-dimensional elasto-plastic beam elements. In order to represent the hysteretic behavior of reinforced concrete members, each element incorporates three sub-elements: (i) an elasto-plastic one to represent the elastic behavior of the member itself, with nonlinear plastic segments at both ends, of varying length depending on the load history; (ii) a connection sub-element to characterize the localized relative rotation at the ends as a result of degradation of steel anchorage; and (iii) a shear sub-element to describe the distortion at critical regions of the member and the shear slip at the ends. Only the effect of the elasto-plastic sub-elements has been considered in this work.

The plastic behavior during loading and unloading is assumed concentrated at the extremes of the member. The stiffness of these plastic zones is represented by an effective average stiffness pEI, with the parameter p and the length of the plastic zone calculated from the moment–curvature history at the extremities.

The moment–curvature relationship M–φ for a given reinforced concrete cross-section is constructed, for a constant axial force, using the following hypotheses: (a) plane sections remain plane during deformation, and normal to the deformed axis of the member; (b) Mander's models [11] are utilized as the constitutive relations for concrete and steel. The cross-section is subdivided in strips parallel to the neutral axis and, for each increment in curvature, the position of the deformed (rotated) cross-section is adjusted iteratively until equilibrium is achieved between the internal and external actions, with the corresponding moment finally calculated.

Fig. 1 shows a member of stiffness EI and EA, between nodes i and j, with reduced end stiffness associated with the factors p_i and p_j. These factors and the length of the end sections are calculated at each step using a moment–curvature hysteretic relationship with parameters also shown in Fig. 1. The factors p_i, p_j satisfy the following rules: (a) $p = 1$, for elastic behavior, (b) $p = h$ for strain hardening, (c) $p = s$ for strain softening, with $z_i = l_p$ (a characteristic length $\cong 0.75d$, d being the cross-sectional depth), (d) $p = 1$ for unloading, (e) $p = 2/(1/r + 1)$ for re-loading, a value obtained from the average of the stiffness corresponding to the extreme section, rEI, and that corresponding to the elastic section EI. The parameters M_y, M_m, EI, h, s, for the positive and negative directions, are calculated by linearization of the relationship M–φ, obtained in a pre-processing of the cross-section.

This formulation has been implemented in the analysis program DINLI [9].

The structural model also incorporates a consistent mass matrix and a viscous damping matrix proportional to the mass and the initial stiffness matrices. The resulting system of equations is solved implementing a Lagrangian incremental scheme, following the Newmark method and, at each step, Newton–Raphson iterations to achieve equilibrium between the internal and external actions for the member.

The analysis allows the determination of the structural response parameters of relevance to the definitions of the limit states for each of the specified performance levels.

1.2. Approximation of the responses via neural networks

When there is no explicit relationship between input and output, it is convenient to represent the relationship by means of a response surface adjusted to a set of deterministic, discrete results. The response surface representation facilitates the estimation of reliability and makes feasible the application of direct Monte Carlo simulation, even with a large sample size. Different types of response surfaces have been discussed in the literature, from global approximations using analytic, quadratic functions [12–14,9,15], to local interpolation [16]. It may be difficult to represent adequately the discrete input-response results with global functions over the full range of the variables and, although local interpolation may offer a better representation, it does so at an increased computational effort.

Among alternative approaches for the representation of an input–output relationship, a response surface using a neural network, trained with an a-priori obtained discrete database, offers flexibility, efficiency and adaptability [5,17–22].

A neural network estimate $F(\mathbf{X})$ for the response $R(\mathbf{X})$ is a general algorithm of the form

$$R(\mathbf{X}) \cong F(\mathbf{X}) = h\left(\sum_{k=0}^{J} W_{kj} h\left(\sum_{i=0}^{N} W_{ji} X_i\right)\right) \tag{1}$$

in which $R(\mathbf{X})$ is the response obtained with the nonlinear dynamic analysis for the input variables X_i, $F(\mathbf{X})$ is the neural network

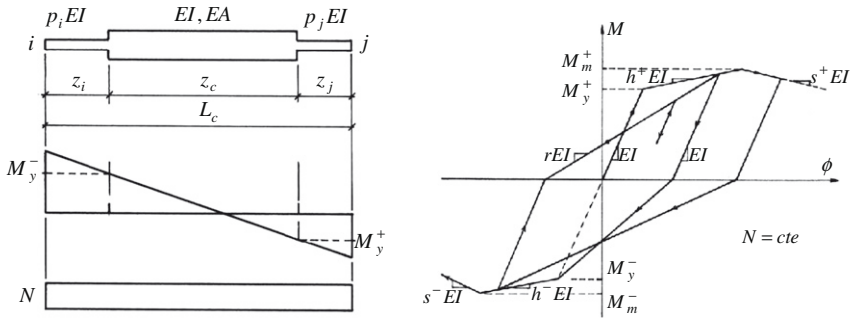

Fig. 1. Bar element and moment–curvature hysteresis.

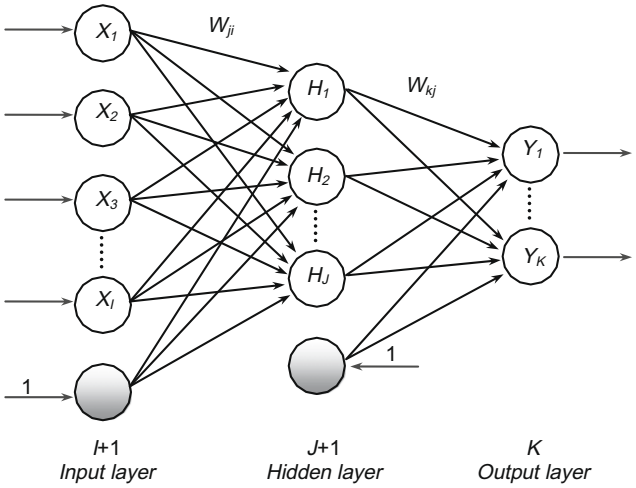

Fig. 2. Schematic for a multi-layer neural network.

approximation, $h(t)$ is a specified transfer function and W_{kj}, W_{ji} are constant weights. The network is schematically represented in Fig. 2, which shows an input layer with N neurons connected to J neurons in an intermediate or "hidden" layer. The input to the j neuron of this layer is contributed by each of the i neurons in the input layer, each with a value X_i and a weight W_{ji}. The total resulting input to each hidden neuron is processed via the transfer function h (usually a sigmoid), before being transmitted to the next, output layer, utilizing the weights W_{kj}. The total resulting inputs to the output neurons are finally processed again via the transfer function h to produce the final results for the K output neurons.

In this work neural networks with a single intermediate or hidden layer are used, and with only one neuron in the output ($Y = F(\mathbf{X})$). The number of neurons in the hidden layer could vary between one and a maximum controlled by the number of input variables and number of data. Given this information, an optimum number of neurons is calculated during the training.

The training process implies finding the weights W to minimize the total error between the network predictions and the information for a data set corresponding to different combinations of the input variables X_i. The complete data set is divided into a training set and one used for validation. Total error is the sum of that calculated over the training set plus that corresponding to the validation set. The total error is calculated for networks with different number of neurons in the hidden layer, choosing the number corresponding to the least total error.

1.3. Discrete database: ranges for structural variables and for ground motions

To generate an input database for neural network training, the dynamic analysis is run for a set of combinations of the intervening variables and design parameters. The application example in this paper uses a portal frame as shown in Fig. 3.

The responses of interest (e.g., the maximum inter-story drift) depend on geometric and structural parameters: the number of stories NS; the number of bays NB; the span XL of each bay; the mass m per unit length associated with each story; the characteristic strength of concrete, f'_c; the width of beams b_b, the depth of beams h_b, the width of columns b_c, the depth of the columns h_c and the steel reinforcement ratios in beams and columns.

In order to develop a general database for this type of structure, the variable ranges used were: NS from 3 to 10; NB from 1 to 4; XL from 300 to 600 cm (all bays had the same span); m from 2.15×10^{-4} to 4×10^{-4} KN s^2/cm^2; f'_c from 20 to 40 MPa; b_b from 15 to 30 cm; h_b from 40 to 70 cm; b_c from 20 to 40 cm; and h_c from 40 to 100 cm. The modulus of elasticity of the concrete was taken as $E_c = 4700\sqrt{f'_c}$. The steel properties, on the other hand, were adopted to be 420 MPa for the yield strength f_y and 200,000 MPa for the modulus of elasticity E_s.

The concrete and steel properties were assumed to be lognormally distributed. Randomly selected values of these properties were then used, during simulations, to calculate the parameters of the moment–curvature relationship shown in Fig. 1.

Steel reinforcement ratios followed code requirements ([23], reproduced from guidelines in New Zealand and from the American Concrete Institute) and obeyed the following ranges: for beams at midspan, ρ_{sb}, from $\sqrt{f'_c}/(4f_y)$ to $(f'_c + 10)/(6f_y)$; over the supports, ρ'_{ss}, from $\sqrt{f'_c}/(4f_y)$ to $(f'_c + 10)/(6f_y)$; for columns, ρ_{sc}, from 0.008 to 0.04286.

The range for the normalized confinement pressure f_r/f'_{c0} was taken from 0.0 to 0.15. Furthermore, when choosing the steel reinforcement ratios, it was verified that they were sufficient to provide adequate strength against gravitational loads.

The dimensions of the beams and columns were assumed to change with the height and the number of stories, as specified in Table 1.

The ground motion requires information on the form of the acceleration record as well as its peak a_g. Responses were obtained

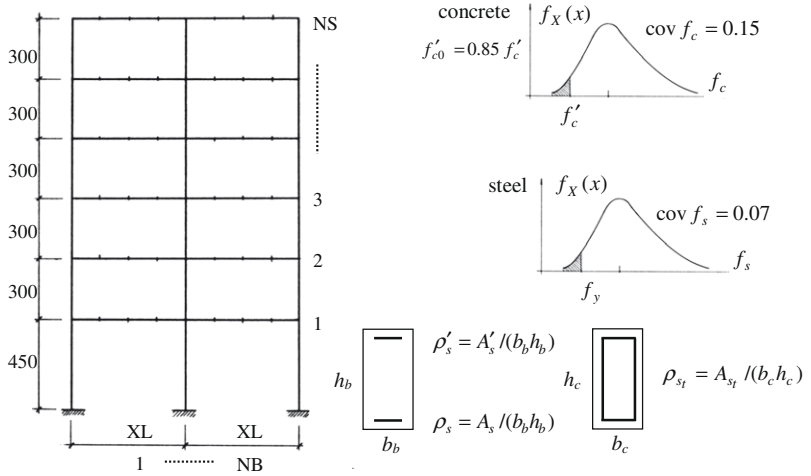

Fig. 3. Variables for the portal frames.

Table 1
Beam and column dimensions in terms of number of stories.

NS	Number of stories with type G1	Number of stories with type G2	Number of stories with type G3
3	2	1	
4	2	2	
5	3	2	
6	3	3	
7	3	2	2
8	3	3	2
9	3	3	3
10	4	3	3

Dimensions per type: G1: b_b, h_b b_c, h_c; G2: b_b, $0.8h_b$ b_c, $0.8h_c$; G3: b_b, $0.6h_b$ b_c, $0.6h_c$.

for 9 peak ground accelerations ranging from 25 to 1200 cm/s^2. Accelerograms were generated as described in [24], following the procedure in [25], using soil filter central frequencies f_g from 2.0 to 3.0 Hz and modifying the results with a modulation function. The accelerograms were then scaled to the desired peak acceleration.

For each a_g, and within the ranges for the remaining variables, 100 different combinations were constructed. Thus, a total of 900 combinations were used. For each one, five sub-combinations were generated, each corresponding to a different earthquake record for the site and to a different combination of parameters in the hysteretic moment–curvature relationship for the members. Five sub-combinations have been used in this paper only as an example, as any larger number of earthquake records could have been included. The nonlinear dynamic analysis was run for each of the five sub-combinations, obtaining from each run the following responses: (1) the maximum lateral displacement u_{max} at the top of the structure; (2) the maximum inter-story drift *DSIM*; (3) the maximum local [26] damage index *DILOM*; and (4) a global damage index *DIG*. Calculations of *DILOM* and *DIG* are described in [24].

For each of the 900 combinations, the mean $\overline{R}_i$ and the standard deviation σ_{R_i} of the response parameters R_i were obtained over the $N = 5$ sub-combinations (i.e., over the set of earthquake records and hysteretic properties). Thus,

$$\overline{R}_i = \frac{1}{N}\sum_{k=1}^{N} R_{k_i} \quad \sigma_{R_i} = \sqrt{\frac{1}{N-1}\sum_{k=1}^{N}(R_{k_i} - \overline{R}_i)^2} \tag{2}$$

These results were organized into two databases with 900 components each, and were used to train two neural networks: one for the mean and the other for the standard deviation of the responses over the variables in the sub-combinations.As it will be discussed in Section 2.1, Eq. (14), the mean and standard deviations were used in combination with lognormal distributions to represent the variability over the earthquake records. Using the sample results for $N = 5$ to represent the underlying, "true" variability is, of course, an approximation. The influence of the number of samples was investigated for a particular combination (7 stories, 2 bays, a_g = 800 cm/s^2, all other variables at their mean), for $N = 5$, 20 and 50 and for the maximum inter-story drift *DSIM*. Because the range covered by $N = 5$ samples was close to the range corresponding to $N = 50$, the fitted lognormal distributions were quite similar to each other, as shown in Fig. 4. With this precaution, and to shorten the computational effort for the presentation of the approach, the sample size $N = 5$ was used throughout.

1.4. Neural networks training results

Neural networks were trained for the two response databases. As an example, Fig. 5 shows the agreement achieved between the actual maximum inter-story drift responses *DSIM* from the dynamic analysis and those predicted using the corresponding neural network.

For perfect agreement, all points would need to fall on the 45° line.

A dispersion due to lack of fit is observed, more for the standard deviation than for the mean, and can be quantified using the standard deviation of the relative error,

$$\sigma_{\varepsilon r} = \sqrt{\frac{1}{N_E - 1}\sum_{k=1}^{N_E}\left(\frac{T_k - Y_k}{Y_k}\right)^2} \tag{3}$$

in which Y_k is the value calculated with the neural network, T_k corresponds to the nonlinear dynamic analysis and N_E = 900, the number of combinations in the database. Eq. (3) can be used to quantify the dispersions $\sigma_{\varepsilon m}$ and $\sigma_{\varepsilon\sigma}$ associated with the neural networks for *DSIM*. Similar analyses were applied to the other response parameters. Thus, using Eq. (3), the mean response $\overline{R}_i$ and the standard deviation σ_{R_i} for each response may be written as Normal distributions around the corresponding values calculated from the networks,

$$\overline{R}_i = \overline{Y}_i(1 + \sigma_{\varepsilon m}X_{N_1}) \quad \sigma_{R_i} = \sigma_{Y_i}(1 + \sigma_{\varepsilon\sigma}X_{N_2}) \tag{4}$$

in which $\overline{Y}_i, \sigma_{Y_i}$ are the mean and standard deviations calculated with the corresponding neural networks and X_{N_1}, X_{N_2} are independent Standard Normal variables.

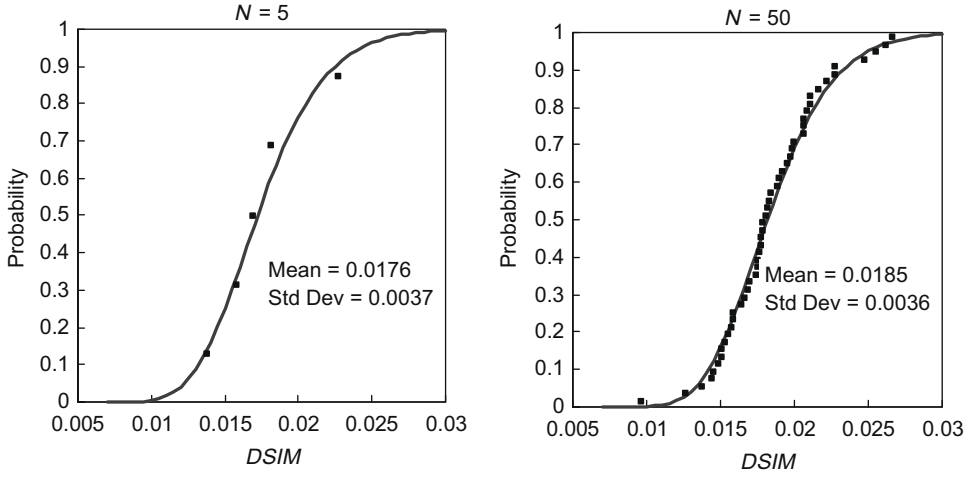

Fig. 4. Lognormal distributions for different sample sizes *N*.

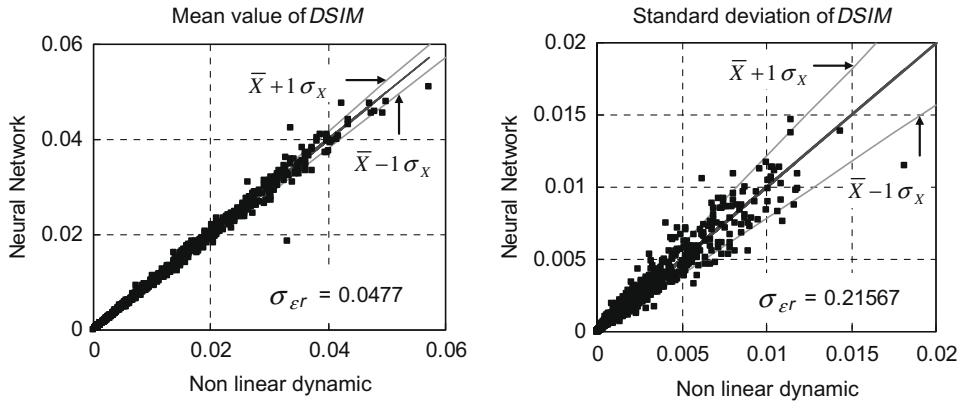

Fig. 5. Neural network training results for $\overline{DSIM}$ and σ_{DSIM}.

2. Reliability estimation

2.1. Performance levels, limit state functions and random variables

In general, limit state functions $G(\mathbf{X})$ are defined in terms of a capacity R_{LIM} and a demand $R(\mathbf{X})$,

$$G(\mathbf{X}) = R_{LIM}(\mu, \delta) - R(\mathbf{X}) \tag{5}$$

in which $R_{LIM}(\mu, \delta)$ represents the limiting value for the response parameter $R(\mathbf{X})$ at a given performance level, with a mean μ and a coefficient of variation δ. The limit state functions considered for the three performance levels were:

- *Operational*
  - Elastic behavior

$$G_{11}(\mathbf{X}) = (\bar{u}_y, 0.10) - u_{\max}(\mathbf{X}) \tag{6}$$

  - Max. inter-story drift

$$G_{12}(\mathbf{X}) = (0.005, 0.10) - DSIM(\mathbf{X}) \tag{7}$$

- Life Safety
  - Max. Inter-story drift

$$G_{21}(\mathbf{X}) = (0.015, 0.10) - DSIM(\mathbf{X}) \tag{8}$$

  - Max. Local Damage Index

$$G_{22}(\mathbf{X}) = (0.60, 0.10) - DILOM(\mathbf{X}) \tag{9}$$

  - Global Damage Index

$$G_{23}(\mathbf{X}) = (0.40, 0.10) - DIG(\mathbf{X}) \tag{10}$$

- *Collapse*
  - Max. Inter-story drift

$$G_{31}(\mathbf{X}) = (0.025, 0.10) - DSIM(\mathbf{X}) \tag{11}$$

  - Max. Local Damage Index

$$G_{32}(\mathbf{X}) = (1.00, 0.10) - DILOM(\mathbf{X}) \tag{12}$$

  - Global Damage Index

$$G_{33}(\mathbf{X}) = (0.80, 0.10) - DIG(\mathbf{X}) \tag{13}$$

Numbers in parentheses indicate corresponding means and coefficients of variation. For G_{11}, $\bar{u}_y$ is the mean yield displacement for the frame, estimated according to [27], below which the structure remains elastic.

Each performance function was further developed by representing the variability, over the sub-combinations, of each demand $R(\mathbf{X})$. For example, for the maximum inter-story drift, when $R(\mathbf{X}) = DSIM(\mathbf{X})$, the variability was represented by a lognormal distribution:

$$R(\mathbf{X}) = \frac{\overline{R}(\mathbf{X})}{\sqrt{1+\left(\frac{\sigma_R(\mathbf{X})}{\overline{R}(\mathbf{X})}\right)^2}} \exp\left[R_{N_1}\sqrt{\ln\left(1+\left(\frac{\sigma_R(\mathbf{X})}{\overline{R}(\mathbf{X})}\right)^2\right)}\right] \tag{14}$$

in which R_{N1} is a Standard Normal variable and the mean $\overline{R}(\mathbf{X})$ and standard deviation $\sigma_R(\mathbf{X})$ are obtained using Eq. (4) and the corresponding neural network representations.

The variability for the maximum local damage index $DILOM(\mathbf{X})$, and for the global damage index $DIG(\mathbf{X})$, both being bounded between 0 and 1, was represented by Beta distributions with the same bounds and corresponding mean and standard deviations $\overline{R}(\mathbf{X})$ and $\sigma_R(\mathbf{X})$. In order to calculate an individual $R(\mathbf{X})$ from the Beta distribution, a random variable R_{N2}, uniformly distributed between 0 and 1, was correspondingly introduced.

The limiting capacities R_{LIM} were also considered random, as shown in Eqs. (6)–(13). The capacity associated with the maximum displacement $u_{max}(\mathbf{X})$, and that for the maximum inter-story drift $DSIM(\mathbf{X})$, were assumed to be lognormally distributed, requiring the introduction of Standard Normal variables R_{N3} as per Eq. (14). Capacities for the maximum local or global damage indices were assumed to obey Beta distributions between 0 and 1, requiring the introduction of random variables R_{N4} uniformly distributed between 0 and 1.

The portal frame example studied in this paper had 6 stories and 3 bays, with inter-story column lengths as shown in Fig. 3. Ground motion characteristics corresponded to those expected for the city of Mendoza, Argentina. Statistics and probability distributions used for all the remaining variables are shown in Table 2.

The coefficients of variation for the variables in this table were chosen to represent realistic values. For example, some of them have a nominal value of 10% (e.g., the mass m). The peak ground acceleration a_G, on the other hand, has a very large variability corresponding to the seismicity of the site. When the variability was small the distribution was assumed Normal. However, some variables that need to be positive (like concrete strength f'_c and steel reinforcement ratios) were assumed to be lognormals. The peak ground acceleration, as it is common in most attenuation relationships, was assumed to also follow a lognormal distribution. Damage parameters are bound by 0 and 1, and were therefore assumed to follow corresponding Beta distributions.

In this table, the symbol ? indicates a design parameter (beam and column depths, and steel reinforcement ratios), the mean values of which will be the output of the subsequent design optimization.

Table 2
Statistics for random variables.

Variable	$\overline{X}$	σ_X	Type	Variable	$\overline{X}$	σ_X	Type
$X(1) = NS$	6	0	Normal	$X(13) = f_r/f'_{c0}$	0.10	0.01	Normal
$X(2) = NB$	3	0	Normal	a_G	$a_G = X(14)\,[1.0+X(15)]$		
$X(3) = XL$	400 cm	20.0 cm	Normal	$X(14) = \bar{a}_G$	94 cm/s^2	130 cm/s^2	Lognormal
$X(4) = m$	2.5×10^{-4}	2.5×10^{85}	Normal	$X(15) = \sigma_{a_G}$	0	0.25	Normal
$X(5) = f'_c$	30 MPa	3 MPa	Lognormal	$X(16) = f_g$	2.50 Hz	0.375 Hz	Normal
$X(6) = b_b$	20 cm	1 cm	Normal	$X(17) = X_{N1}$	0	1	Normal
$X(7) = h_b$	? cm	$0.05\,\overline{X}$	Normal	$X(18) = X_{N2}$	0	1	Normal
$X(8) = b_c$	30 cm	1.5 cm	Normal	$X(19) = R_{N1}$	0	1	Normal
$X(9) = h_c$	? cm	$0.05\,\overline{X}$	Normal	$X(20) = R_{N2}$ (*)	0	1	Uniform
$X(10) = \rho_{sb}$	?	$0.10\,\overline{X}$	Lognormal	$X(21) = R_{N3}$	0	1	Normal
$X(11) = \rho_{ss}$	?	$0.10\,\overline{X}$	Lognormal	$X(22) = R_{N4}$ (*)	0	1	Uniform
$X(12) = \rho_{sc}$	?	$0.10\,\overline{X}$	Lognormal	(*) Bounds for Uniform distribution			

2.2. Probability of non-performance or failure

For each of the three performance levels considered, the non-performance or failure probability Pf can be calculated as:

$$Pf = \text{Prob}[G(\mathbf{X}) \leqslant 0] \tag{15}$$

utilizing a standard Monte Carlo simulation, simultaneously including all limit state functions in the performance level, according to Eqs. (6)–(13), as in a series system.

The number of replications used varied between 10^6 and 10^7, a task significantly facilitated by the use of neural networks for the structural responses $R(\mathbf{X})$. In all cases, the number of replications chosen resulted in a coefficient of variation not greater than 3% for the distribution of the probability estimate. In some cases, a smaller number of replications could have been used. However, computer speed and the benefit of using the neural network representation made it superfluous to seek, in each case, the appropriate smaller replication size. The non-performance probability thus calculated is conditional on the occurrence of an earthquake. An annual probability is obtained by taking into account the occurrence of earthquakes as a Poisson arrival process. For the city of Mendoza, earthquakes with magnitudes $M \geqslant 5$ have a mean arrival rate $\nu = 0.20$. Accordingly, the annual probability of non-performance Pf_{annual} at each level can be estimated from

$$Pf_{annual} = 1. - \exp[-\nu Pf] \rightarrow \beta_{annual} \cong -\Phi^{-1}(Pf_{annual}) \tag{16}$$

which can be expressed as an associated reliability level β_{annual}, as shown in Eq.(16), using the Normal distribution Φ.

2.3. Neural network representation of calculated reliabilities

In order to make more efficient the optimization process implied by performance-based design, to be described in the following section, discrete databases were obtained for the reliability indices β_1, β_2, β_3 corresponding to the three performance levels. Thus, for different combinations of the design parameters d_i, shown in Table 3, the reliability levels were computed as previously discussed and then used to train three corresponding neural networks. The input vectors to these networks are the design parameters.

Table 3
Design parameters.

Variable	$\overline{X}$	σ_X	Type
$X(7) = h_b = d_1$	? cm	$0.05\,\overline{X}$	Normal
$X(9) = h_c = d_2$	? cm	$0.05\,\overline{X}$	Normal
$X(10) = \rho_{sb} = d_3$	?	$0.10\,\overline{X}$	Lognormal
$X(11) = \rho'_{ss} = d_4$	?	$0.10\,\overline{X}$	Lognormal
$X(12) = \rho_{sc} = d_5$	?	$0.10\,\overline{X}$	Lognormal

The advantage of this approach is that, during the optimization process, the evaluation of the achieved reliabilities can be done by executing the trained networks rather than using each time a Monte Carlo simulation.

Fig. 6 shows a comparison between reliabilities calculated with the trained networks and those obtained with the simulation process previously described, for each of the performance levels. Again, a small dispersion is observed, which could be accounted for as previously discussed for the structural responses. Fig. 6 shows, in each case, the standard deviation of the relative training error.

3. Optimization and performance-based design

3.1. The problem

The optimization problem is defined as follows: given an objective function $F(\mathbf{d})$, with $\mathbf{d}$ being the vector of design parameters, obtain an optimum $\mathbf{d}$ corresponding to a minimum F, while maintaining minimum target reliability levels β_i ($i = 1, M$) for each of M performance levels. The objective function could be, for example, the structural weight. In this work, it is chosen to be the total cost of the structure, including the initial construction cost plus that of damage repair or replacement following the occurrence of an earthquake.

The design parameters can be defined as the mean values or the standard deviations of some of the random variables in the problem. In this case, the parameters are chosen to be the mean values of the beam and column depths h_b and h_c, and the mean values of the steel reinforcement ratios ρ_{sb}, ρ_{ss} and ρ_{sc}.

3.2. Optimization strategy

The optimization problem can be approached with a variety of algorithms in the literature [28]. Some of these (quasi-Newton methods) require the calculation of the gradient of the objective function, others (search-based or genetic algorithms) only require the calculation of the function itself. The latter also simplify the problem of incorporating inequality constraints, as introduced in our case by the minimum reliability requirements.

Thus, in this work, a search scheme is used and is described as follows.

(a) A set of initial combinations of the design parameters are chosen randomly, within specific bounds for each parameter.
(b) The reliability levels at each performance level are calculated for each initial combination, using either Monte Carlo simulation and the structural responses' neural networks, or using directly the reliability indices' neural networks.

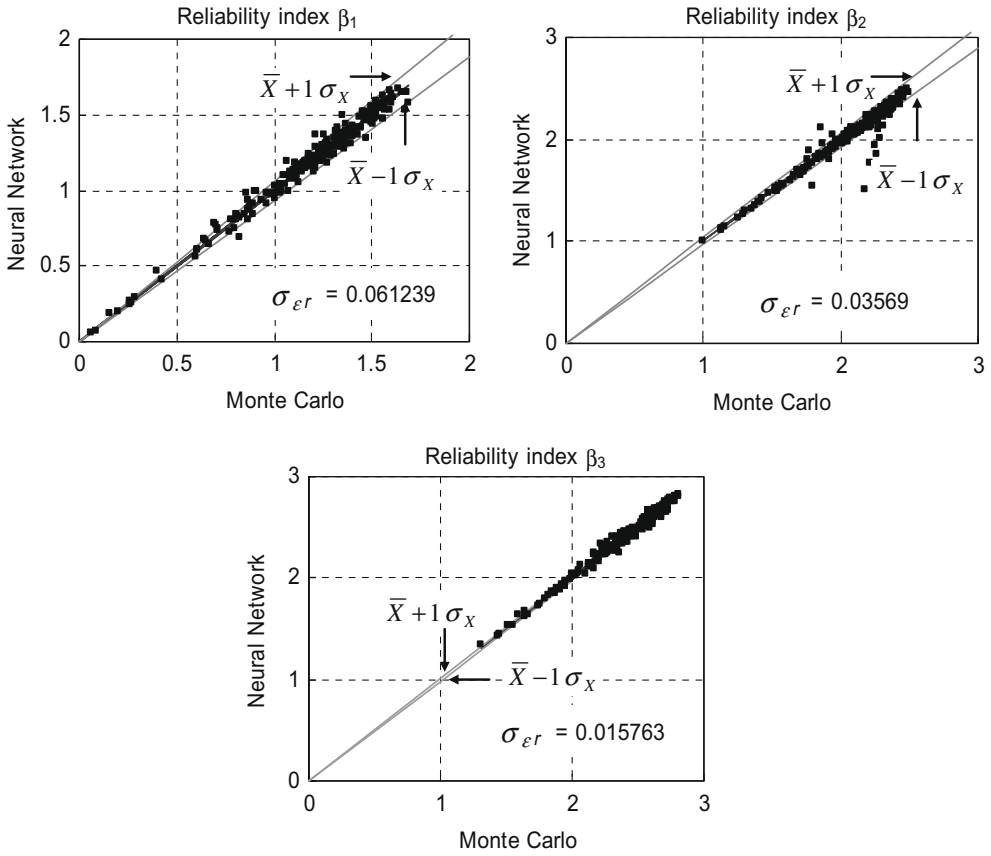

Fig. 6. Neural networks training results for reliability indices,three performance levels.

(c) The objective function is evaluated for those combinations satisfying the minimum target reliabilities, choosing the combination that produces the minimum objective value. This combination is taken as the "initial anchor point".
(d) A new set of combinations is chosen randomly within a sphere with the anchor point at its center. The reliability level is calculated for each combination, and the objective function is evaluated only for those combinations satisfying the minimum target reliabilities. Should an objective function be found lower than the value at the anchor, that combination is chosen as the "updated anchor". The process is repeated around this new anchor.
(e) The process is continued until all combinations within the sphere, satisfying the reliability constraints, lead to an objective function greater or equal than that for the current anchor. The corresponding anchor combination is taken as an approximation to that for the minimum.
(f) The process is repeated from the beginning, choosing a different random start for a new cycle. Different initial conditions may lead, in general, to different minima. This would be the case should the problem accept different minima. If there is only one optimum, then the differences between the minima would be small and within the numerical tolerances used. The final optimum is taken as the combination corresponding to the lowest minimum.

This simple scheme avoids possible numerical problems associated with the calculation of gradients, and its efficiency is incremented through the use of neural networks for the calculation of either structural responses or achieved reliabilities. The process scheme is shown in Fig. 7.

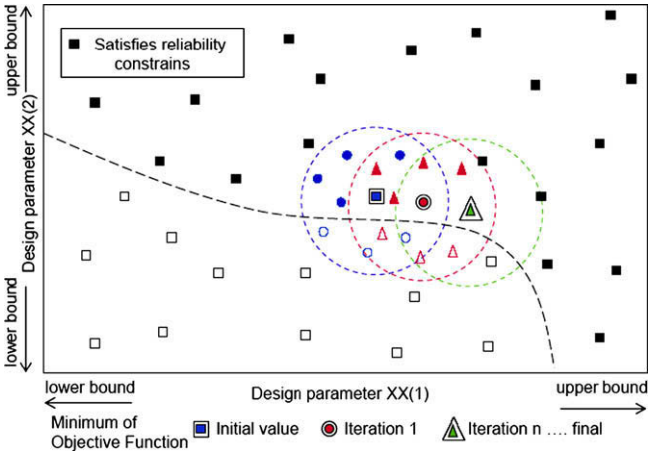

Fig. 7. Optimization process.

The computational demands may be lower when the reliabilities are obtained from the corresponding neural networks than when they are calculated by simulation at each step, even when neural networks are used for the structural responses. In the first case, simulations are only used to develop the discrete reliability database.

4. Numerical results

4.1. Design parameters and target minimum reliabilities

The design parameters shown in Table 3 were constrained to be within the following bounds: depth of beams h_b from 40 to 70 cm;

Table 4
Target annual and event probabilities.

Performance level	Pf_{annual}	β_{annual}	Pf	β
Operational	2×10^{-2}	2.054	0.10101	1.276
Life safety	2×10^{-3}	2.878	0.10010×10^{-1}	2.326
Collapse	7×10^{-4}	3.195	0.35012×10^{-2}	2.697

depth of the columns h_c from 40 to 100 cm. The steel reinforcement ratios obeyed the bounds described in Section 1.3.

Target reliabilities are given for annual minima, which can be converted to event targets using Eq. (16). The minimum annual target probabilities used, and the corresponding event probabilities and reliability indices are shown in Table 4. These followed recommendations by [29].

4.2. Objective function: total cost

The objective function adopted here is the total structural cost, including that for initial construction plus that associated with repairs or replacement after an earthquake and different levels of damage. The latter must take into account the probability that the earthquake would occur during the service life.

4.2.1. Initial cost

The unit cost of concrete includes materials, forming and labor, and is assumed to be $CUC = 300$ \$/m^3 (in US dollars for Argentine conditions).

The unit cost of steel, including the material and installation labor, is assumed to be $CUS = 120$ \$/KN.

In terms of the random variables in the problem, the concrete volume results

$$\begin{aligned} Vol(\mathbf{X}) &= V_{beams} + V_{columns} \\ &= \left[\overline{X}(1)\overline{X}(2)\overline{X}(3)\overline{X}(6)\overline{X}(7)0.9 \right. \\ &\quad \left. + (150 + 270\overline{X}(1))(1 + \overline{X}(2))\overline{X}(8)\overline{X}(9)\right]10^{-6}m^3 \end{aligned} \tag{17}$$

or

$$Vol(\mathbf{d}) = [145,800 \cdot \overline{X}(7) + 212,400 \cdot \overline{X}(9)]10^{-6}m^3$$

in terms of the design parameters. The steel weight, including an approximate contribution from stirrups, results

$$\begin{aligned} P(\mathbf{X}) &= [V_{beams}(\rho_{sb} + 0.6\rho'_{ss} + 0.0065) + V_{columns}(\rho_{sc} + 0.009)]78.5KN \\ &= \left[V_{beams}(\overline{X}(10) + 0.6\overline{X}(11) + 0.0065) \right. \\ &\quad \left. + V_{columns}(\overline{X}(12) + 0.009)\right]78.5KN \end{aligned}$$

or

$$\begin{aligned} P(\mathbf{d}) = &\left[0.1458X(7)(\overline{X}(10) + 0.6\overline{X}(11) + 0.0065) \right. \\ &\left. + 0.2124X(9)(\overline{X}(12) + 0.009)\right]78.5KN \end{aligned} \tag{18}$$

in terms of the corresponding design parameters. The initial cost of the portal frame is, therefore,

$$C_0 = Vol(\mathbf{d})CUC + P(\mathbf{d})CUS \tag{19}$$

4.2.2. Repair or replacement cost

The future repair cost, at present values, depends on (1) the level of damage caused by the earthquake, (2) when this event occurs within the lifetime of the structure, and (3) the discount rate available to accumulate repair funds until needed.

Here the global damage index *DIG* is used as an indicator of structural distress. If $C_f(DIG)$ is the cost function in terms of this *DIG* occurring at a time t, then the present cost $C_{f0}(DIG)$ at $t = 0$, r being the discount rate, is

$$C_{f0}(DIG) = C_f(DIG)\exp(-rt) \tag{20}$$

When the arrival of earthquakes is simulated as a Poisson process, the probability of an earthquake occurring at time t is

$$P(t \leqslant T_1 \leqslant t + dt) = f(t)dt = v\exp(-vt)dt \tag{21}$$

and, therefore, the expected present cost, conditional on the damage *DIG*,

$$C_1|_{DIG} = \int_0^\infty C_{f0}(DIG)f(t)dt = C_f(DIG)\frac{v}{r+v} \tag{22}$$

This relationship has been developed by [30]. In this application, the relationship between damage level *DIG* and repair cost is assumed to be

$$\begin{aligned} &C_f(DIG) = \alpha C_0\left(\frac{DIG}{0.60}\right)^b \quad \text{if} \quad DIG \leqslant 0.60 \\ &C_f(DIG) = \alpha C_0 \quad \text{if} \quad DIG > 0.60 \end{aligned} \tag{23}$$

in which C_0 is the complete replacement cost, with $\alpha = 1.20$ assumed to be a factor to account for demolition and clearing. Eq. (23) assumes that complete replacement will take place when *DIG* exceeds 0.60. For damage levels lower than 0.60 the cost could increase in general with an exponent b, although in this work $b = 1$ has been used. Additional damage-related costs, like insurance premiums, service interruption, etc., should also be taken into account but have not been included in this example.

Finally, the total expected cost of repair is

$$C_1 = \int_0^1 C_1|_{DIG} \cdot f_{DIG}(DIG) \cdot d(DIG) \tag{24}$$

using the probability density function for the index *DIG*. This can be obtained by first obtaining the cumulative distribution, using Monte Carlo simulation and the neural networks for the response *DIG*, adjusting a Beta distribution and subsequently obtaining the density function. The objective is the minimization of the total expected cost, $C_1 + C_0$, subject to the minimum reliability constraints in each of the performance levels.

4.3. Results

4.3.1. Using Monte Carlo simulations to estimate reliability at each step of the optimization process

Optimization results for this case are shown in Table 5. Three cycles were executed during the optimization process, corresponding to three different initial choices for design parameters.

The minima corresponding to the three cycles were quite similar, but with somewhat different values for the design parameters. The overall minimum, for cycle 3, shows an intermediate initial cost but lower repair cost, highlighting the importance of addressing both types of cost in the analysis. The optimization, with intermediate reliabilities estimated by Monte Carlo simulation using the response neural networks, used 225 simulations with 500,000 replications each to complete all three cycles.

4.3.2. Using reliability neural networks at each step of the optimization

The results when the neural networks for reliability are implemented in the optimization are shown in Table 6.

With this strategy, the results for the first and third cycle are quite similar to those respectively shown in Table 5. Here the optimum results correspond to the second cycle, with a combination of beam and column dimensions very similar to those of the first. The initial cost for the first cycle is greater, however, due to higher steel ratios, resulting also in lower repair costs. The optimum second cycle, however, has higher repair costs, but not sufficiently high to mask the initial savings in steel.

Table 5
Results when reliability estimated by simulation at each optimization step.

Design parameter	Cycle 1	Cycle 2	Cycle 3
$d_1 = \overline{X}(7) = h_b$ (cm)	59.18	62.65	59.95
$d_2 = \overline{X}(9) = h_c$ (cm)	53.73	58.15	50.13
$d_3 = \overline{X}(10) = \rho_{sb}$	0.01117	0.00904	0.01024
$d_4 = \overline{X}(11) = \rho'_{ss}$	0.01211	0.01287	0.01145
$d_5 = \overline{X}(12) = \rho_{sc}$	0.02124	0.01747	0.02624
Initial cost ($)	10,777	11,000	10,818
Repair cost ($)	1638	1496	1471
Total cost ($)	12,415	12,496	12,289
β_1 (β_{1T} = 1.276)	1.4400	1.4710	1.4296
β_2 (β_{2T} = 2.326)	2.3512	2.3726	2.3508
β_3 (β_{3T} = 2.697)	2.7027	2.7059	2.7031

β_{1T}, β_{2T} and β_{3T} correspond to the minimum target levels for the corresponding performance levels.

Table 6
Results when using reliability neural networks at each optimization step.

Design parameter	Cycle 1	Cycle 2	Cycle 3
$d_1 = \overline{X}(7) = h_b$ (cm)	60.41	59.76	61.23
$d_2 = \overline{X}(9) = h_c$ (cm)	53.10	53.06	50.71
$d_3 = \overline{X}(10) = \rho_{sb}$	0.01226	0.01171	0.00782
$d_4 = \overline{X}(11) = \rho'_{ss}$	0.01366	0.01270	0.01310
$d_5 = \overline{X}(12) = \rho_{sc}$	0.01916	0.01782	0.02447
Initial cost ($)	10,712	10,436	10,665
Repair cost ($)	1286	1419	1280
Total cost ($)	11,998	11,855	11,945
β_1(β_{1T} = 1.276)	1.4179	1.4062	1.4560
β_2(β_{2T} = 2.326)	2.3304	2.3306	2.4050
β_3(β_{3T} = 2.697)	2.7098	2.7006	2.7148

β_{1T}, β_{2T} and β_{3T} correspond to the minimum target levels for the corresponding performance levels.

Table 7
Results using 10 complete optimization cycles

Design parameter		Initial cost ($)	10,466
$d_1 = \overline{X}(7) = h_b$ (cm)	61.29	Repair cost ($)	1256
$d_2 = \overline{X}(9) = h_c$ (cm)	51.78	Total cost ($)	11,722
$d_3 = \overline{X}(10) = \rho_{sb}$	0.00899	β_1 (β_{1T} = 1.276)	1.4483
$d_4 = \overline{X}(11) = \rho'_{ss}$	0.01294	β_2 (β_{2T} = 2.326)	2.3831
$d_5 = \overline{X}(12) = \rho_{sc}$	0.02383	β_3 (β_{3T} = 2.697)	2.7054

β_{1T}, β_{2T} and β_{3T} correspond to the minimum target levels for the corresponding performance levels.

To generate the reliability database for neural network training, 224 combinations of design parameters were utilized, resulting in an equal number of Monte Carlo simulations for reliability estimation. This number is similar to the number of simulations in the previous strategy. However, the optimization time was substantially reduced, allowing for more cycles to search for possibility of local minima.

Table 7 shows the results when using ten complete optimization cycles. The total cost is reduced to $11,722 from $11,855, a difference of just 1.1%.

It can be concluded that several fairly different combinations of design parameters can lead to similar total costs. The final ''optimum" must then be chosen by the design engineer taking into account other construction constraints.

5. Conclusions

The following conclusions can be offered from the results of this work, as well as suggestions for further research.

- Performance-based design in earthquake engineering implies consideration of the uncertainties in the structural demands and capacities, in order to evaluate the reliability associated with each of the required performance levels. These reliabilities must satisfy minimum target values for each level.
- Calculation of the structural responses for the formulation of the limit states equations requires a nonlinear dynamic analysis, and these responses cannot be given in an explicit relationship in terms of the intervening random variables. Discrete data can be obtained for chosen combinations of these variables, and the results can be expressed in terms of response surfaces or neural networks. In this work the latter approach has been followed, providing flexibility and adaptability.
- The major computational demand in this approach is the construction of the discrete database, executing the nonlinear dynamic analysis for a number of variable combinations representative of the variable ranges. For a fixed combination within a sub-set of the variables, the analysis is carried out for another sub-set which groups variables including different ground motions. For each combination, and over the set of grouped variables, the mean and the standard deviation of each response of interest are obtained. These statistics are then represented by neural networks, and are utilized in representing the responses in a probabilistic manner.
- The utilization of neural networks' representation for the response demands makes feasible the calculation of the probability of non-performance via standard Monte Carlo simulation.
- The reliability associated with each performance level can thus be estimated for different combinations of design parameters, and these reliabilities can themselves be represented by neural networks.
- The optimization in performance-based design implies the minimization of an objective function (here the total structural cost was used) subject to the achievement of minimum target reliabilities at each performance level. This work has shown the implementation of an optimization scheme based on a search without calculation of gradients. This scheme is efficient, whether the intermediate reliability constraints are evaluated by simulation at each step, or they are implemented using the reliability neural networks.
- The optimization scheme for minimum total cost has been applied to a multi-storey, multi-bay reinforced concrete frame, with the design parameters being the depths of beams and columns, and three steel reinforcement ratios. The results show good agreement between the two ways of implementing the calculation of the reliability constraints, and that somewhat different optimum design parameters may correspond to minor differences in the total cost. In particular, the results have shown that it is important the consideration of damage repair costs, as they influence the optimum solution.
- This work has shown that neural networks offer a very useful tool to represent the relationship between structural responses and the intervening random variables, and between achieved reliabilities and the design parameters. The first application make feasible the use of Monte Carlo simulation to estimate reliabilities or probabilities of non-performance, while the second improves the efficiency of the optimization algorithm when intermediate reliabilities need to be evaluated.
- The approach presented introduced a general scheme for reliability estimation and performance-based design optimization in earthquake engineering. It introduced required concepts like a relationship between damage level and repair cost – a relationship that still needs further general development and should be the objective of continuing research.

- Continuing research should also be focused on damage parameters and their relationship to calculated quantities like strains and displacements. Here a well known damage index was used for the purpose of the application, but further research should be focused on how damage accumulates over time as a result of the applied strains or displacement history.

Acknowledgements

This work was conducted with the support from the National University of Rosario, Argentina, to the first author, for the project "Reliability of structural systems under dynamic demands", 1ING 142 (19/I202). Support to the second author was received from the Natural Sciences and Engineering Research Council of Canada, for the project "Neural networks for reliability and performance-based design in earthquake engineering", RGPIN 5882-04, University of British Columbia, Vancouver, Canada. Both supports are gratefully acknowledged.

References

[1] SEAOC Vision 2000 Committee. Performance based seismic engineering of buildings. Sacramento, California, USA: Structural Engineers Association of California; 1995.
[2] FEMA. NEHRP guidelines for the seismic rehabilitation of buildings. Report 273. Buildings Seismic Safety Council; 1997.
[3] Conte J, Durrani A, Shelton R. Seismic response modeling of multi-story buildings using neural networks. J Intell Mater Syst Struct 1994;5(3):392–402.
[4] Beyer W, Liebscher M, Beer M, Graf W. Neural network based response surface methods – a comparative study, in: Proceedings of the 5th German LS-DYNA forum, DYNAmore GmbH, Ulm, 2006.
[5] Hurtado J. Structural reliability – statistical learning perspectives. Lecture notes in applied and computational mechanics, vol. 17. Springer Verlag; 2004.
[6] Brown A, Yang H, Wrobleski M. Improvement and assessment of neural networks for structural response prediction and control. J Struct Eng, ASCE 2005;131(5):848–50.
[7] Tsompanakis Y, Lagaros N, Papadrakakis M. Structural design optimization considering uncertainties. In: Frangopol M, editor. Structures & infrastructures Series, vol. 1. CRC Press, Taylor and Francis; 2008.
[8] Papadrakakis M, Lagaros N. Reliability-based structural optimization using neural networks and Monte Carlo simulation. Comput Meth Appl Mech Eng 2002;191:3491–507.
[9] Möller O. Metodología para evaluación de la probabilidad de falla de estructuras sismorresistentes y calibración de códigos. PhD dissertation. Argentina: Universidad Nacional de Rosario; 2001.
[10] Möller O, Foschi R, Quiroz L, Rubinstein M. Application of neural networks to the optimal seismic design of reinforced concrete frames. In: Proceedings of the ECCOMAS conference on computational methods in structural dynamics and earthquake engineering, COMPDYN07, Crete, Greece, 2007.
[11] Mander JB, Priestley MJN, Park R. Seismic design of bridge piers. Research Report 84-2. New Zealand: Department of Civil Engineering, University of Canterbury; 1984.
[12] Faravelli L. Response surface approach for reliability analysis. J Eng Mech, ASCE 1989;115:2763–81.
[13] Bucher CG, Bourgund U. A fast and efficient response surface approach for structural reliability problems. Struct Saf 1990;7(1):57–66.
[14] Kim S-H, Na S-W. Response surface method using vector projected sampling points. Struct Saf 1997;19:3–19.
[15] Möller O, Foschi R. Reliability evaluation in seismic design: a response surface methodology. Earthquake Spectra 2003;19(3):579–603.
[16] Foschi R, Li H, Zhang J. Reliability and performance-based design: a computational approach and applications. Struct Saf 2002;24:205–18.
[17] Chau KW. Reliability and performance-based design by artificial neural network. Adv Eng Softw 2007;38:145–9.
[18] Zhang J. Performance-based seismic design using designed experiments and neural networks. PhD thesis. Canada; Department of Civil Engineering, University of British Columbia: 2003.
[19] Zhang J, Foschi RO. Performance-based design and seismic reliability analysis using designed experiment and neural networks. Probab Eng Mech 2004;19:259–67.
[20] Möller O, Foschi R, Rubinstein M, Quiroz L. Momento–curvatura de secciones de hormigón armado sismorresistentes utilizando redes neuronales. Mecánica Comput 2006;XXV:2145–62. AMCA.
[21] Möller O, Foschi R, Rubinstein M, Quiroz L. Vulnerabilidad sísmica de estructuras: una aproximación probabilística usando redes neuronales. Memorias XIX Jornadas Argentinas de Ingeniería Estructural, CD, 050, AIE, 2006.
[22] Möller O, Foschi R, Rubinstein M, Quiroz L. Confiabilidad de estructuras sismorresistentes utilizando diferentes aproximaciones de la respuesta dinámica no lineal. Memorias del séptimo encuentro de investigadores y profesionales Argentinos de la construcción VII EIPAC 2007, CD E08-01, 2007.
[23] INPRES-CIRSOC 103. Code for aseismic construction for Argentina, Part II: reinforced concrete; 1991.
[24] Möller O, Foschi R, Rubinstein M, Quiroz L. Seismic structural reliability using different nonlinear dynamic response surface approximations. Struct Saf 2009;31(5):432–42.
[25] Shinozuka M, Sato Y. Simulation of nonstationary random processes. J Eng Mech, ASCE 1967;93(1):11–40.
[26] Park YJ, Ang AH-S. Mechanistic seismic damage model for reinforced concrete. J Struct Eng, ASCE 1985;111(ST4):722–39.
[27] Priestley MJN. Brief comments on elastic flexibility of reinforced concrete frames and significance to seismic design. Bull New Zeal Natl Soc Earthquake Eng 1998;3(4).
[28] Gill PE, Murray W, Wright M. Practical optimization. London, UK: Academic Press; 1993.
[29] Paulay T, Priestley M. Seismic design of reinforced concrete and masonry buildings. New York: John Wiley & Sons; 1992. p. 85.
[30] Sexsmith RG. Bridge risk assessment and protective design for ship collision. In: Proceedings of the colloquium on ship collision with bridges and offshore structures, international association for bridge and structural engineering, IABSE, Copenhagen, 1983.